Sentinel 2 High-Resolution Land Cover Mapping in Sub-Saharan Africa with Google Earth Engine

Sentinel 2 High-Resolution Land Cover Mapping in Sub-Saharan Africa with Google Earth Engine

Elena Belcore[a] and Marco Piras[b]
DIATI, Politecnico di Torino, Corso Duca degli Abruzzi 24, 10129 Torino, Italy

Keywords: Land Cover, Machine Learning, Sentinel-2, Google Earth Engine, Sub-Saharan, Natural Hazard, Climate Change.

Abstract: This work aims to develop an efficient methodology for high-resolution spatial and thematic land cover maps of sub-Saharan areas based on Sentinel-2 data. LC mapping in these areas is complicated due to their land morphology, climatic conditions and homogeneity of surface spectral responses. Two pixel-based supervised classification approaches are compared in Google Earth Engine. The *aggregated* method classifies each image and then aggregates the results on frequency bases at pixel level. The *stacked* method classifies all the images together in a single stacked database. Additionally, the influence of linear atmospheric correction models on the overall accuracy (OA) is assessed, and the best-performing approach is compared to existing Land Cover (LC) maps of the area. 16 Sentinel-2 images (level 1C) from 2017 and 2019 were atmospheric and topographically corrected and classified into nine classes. The results show similar performances for the analysed approaches, with a slightly high OA for the aggregated classification (0.97). The atmospheric correction has little impact on the results.

1 INTRODUCTION

Sub-Saharan Africa is exceptionally vulnerable to Climate Change-induced phenomena, such as floods, erosion, and droughts, which have dramatically increased in the past years. The Dosso region in southwest Niger is no exception (Bigi et al., 2018; Oguntunde et al., 2018; Teodoro and Duarte, 2022). In 2021, 200,000 people were affected by floods in Niger. One of the most recent disastrous events occurred in October 2022, when flooding caused by heavy rains claimed nearly 200 lives and affected more than a quarter of a million people.

In such scenarios, to plan against natural disasters, continuous and detailed monitoring of the area is not negligible (Tiepolo et al., 2018), and updated information regarding the Land Cover (LC) is crucial to land management, as these maps provide users with information related to terrestrial ecosystems and livelihoods (Li et al., 2020). Classification of Sub-Saharan areas is one of the most challenging due to the landscape complexity and the low spectral variability within the covers. Moreover, the sand dust particulates in the atmosphere may alter the spectral response of the Earth surface and further exacerbate the difficulty of the classification. One of the most significant problems in the optical remote sensing of Sub-Saharan regions is that reflectance from soil and rock during the dry season is often much greater than that of the sparse vegetation making it difficult to separate the vegetation. Some specific problems involved with remote sensing of arid vegetation include multiple scattering of light (nonlinear mixing) between vegetation and soil (Huete, 1988). Moreover, the local architecture, such as Nigerienne architecture, consists of tiny houses with flat roofs built using local clays and not plastered, which results in hardly spectral separable build-up areas and bare soils, even from very high resolution (VHR) imagery (Belcore et al., 2022), Figure 1.

Similarly, in some villages and suburbs, the roads are unpaved. As a consequence, the spectral response of buildings is the same as roads and bare soil. The strong seasonality adds further complexity to the classification as the frequent cloud cover during the rainy season and sand presence in the air may alter the spectral values of sensed data.

[a] https://orcid.org/0000-0002-3592-9384
[b] https://orcid.org/0000-0001-8000-2388

Belcore, E. and Piras, M.
Sentinel 2 High-Resolution Land Cover Mapping in Sub-Saharan Africa with Google Earth Engine.
DOI: 10.5220/0011746500003473
In *Proceedings of the 9th International Conference on Geographical Information Systems Theory, Applications and Management (GISTAM 2023)*, pages 27-36
ISBN: 978-989-758-649-1; ISSN: 2184-500X

These reasons contribute to the LC data scarcity in Sub-Saharan Africa. Indeed, to date, few very high-resolution LC maps of sub-Saharan areas exist. Examples are the Africa LC by ESA and FROM-GLC10 (Li et al., 2020). Although these LC maps are incredibly complex to realise, most do not provide good thematic detail. Because of their nature, the training datasets are hardly updatable due to the large amount of time and manual work this task requires.

Figure 1: Aerial view of local architecture acquired by a drone system in 2021.

Niger's southern territories are the study area of the ANADIA 2.0 project (Anadia 2.0, 2023). It aims to create an Early Warning System to face climate change effects in Sirba River Basin in the Tillabery region, enhance local technicians' knowledge regarding floods forecasting, and create an adaptation strategy planform two villages along the Sirba River. In this area, the need for climatic planning and the development of adaptation strategies to climate change at the local level is not negligible (Tiepolo et al., 2018). Despite this undeniable need for climate planning, there is no appropriate risk mapping of the area; indeed, subnational risk mapping lacks detail (Tiepolo et al., 2018). The data gathered and the information provided by this work are directly involved in ANADIA 2.0 by feeding the adaptation strategy plan and investigating the cause-effect relation of floods.

Aiming to map and monitor the areas potentially flooded by the Sirba river, a workflow to produce an updated, high-detailed LC map of the site is proposed and validated. In this application, the LC map of southwest Niger has been realised using nine classes over 16 features. The entire process was completed in the Google Earth Engine (GEE) platform, and two multi-temporal approaches for classification were tested and compared.

2 MATERIALS AND METHODS

2.1 Study Area

Sirba River is a tributary of the Niger River and crosses Burkina Faso and Niger countries (Figure 2). Its basin is prone to floods, and villages along the river are vulnerable to life and economic losses (Massazza et al., 2019, 2018; Tamagnone et al., 2019).

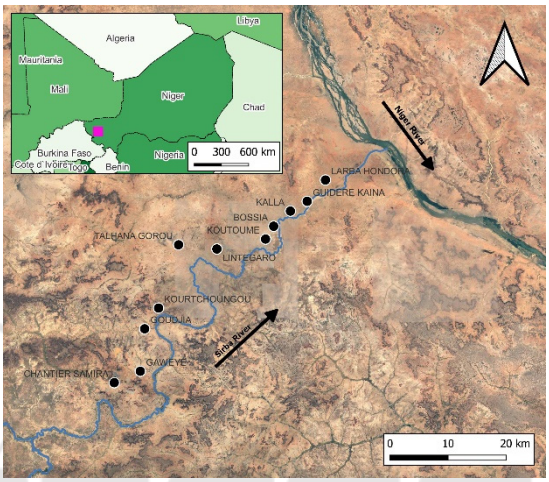

Figure 2: Footprint on the classification (red) and detail of the Nigerienne branch of the Sirba River.

2.2 Identification of Classes

Nine classes describe the classification system, as table 1 illustrates.

2.3 Satellite Imagery Filtering and Pre-Processing

The images acquired by Sentinel-2 (both Sentinel-2A and Sentinel-2B satellites) were filtered by location and date. The study area includes the segment of Sirba River that lies in Niger country for about 100 km. The period covers all the acquisitions between 2017 and 2019. An additional filtering parameter regards the cloud cover percentage, which must be less than 10% over a single scene. Only images sensed during the rainy season (from August to October) were selected to maximise the classes' spectral variability, especially to better distinguish between the vegetation classes and the bare soils and to identify water. Sentinel-2 level 1C dataset was used for this classification since only one image from the corrected dataset of Sentinel-2 level 2A satisfied the filter mentioned above parameters. The selected images of Sentinel 2A-1C level are 16 (Table 2). The

dataset was atmospherically corrected by applying Dark Object Subtraction (DOS) (Chavez, 1988), which is a linear atmospheric correction model that performs similarly to radiative transfer models on homogeneous surfaces (Lantzanakis et al., 2017).

Table 1: Classes of the classification in South Niger.

N	Class	Description	Picture
1	Water	Internal waters	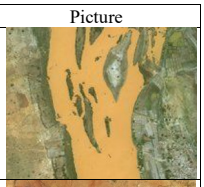
2	Plateaux	Elevated areas over the dry savannah. They influence the water catchment, the erosion process and present peculiar plant species.	
3	Riparian vegetation	The thickly vegetated area along the rivers. It is usually composed of trees and bushes.	
4	Urban areas	Villages and main roads.	
5	Red bare soils	Red soils rich in ferric oxides that characterised the savannah soil landscape.	
6	Sandy bare soils	Sand natural deposits.	
7	Vegetation of the plateaux	Vegetation on the plateaux. It grows along the drainage canals. It is mainly composed of herbaceous species.	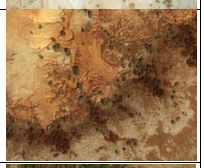
8	Irrigated agricultural lands	Areas interested by intense agricultural activity that require tillage, and irrigated generally through channel systems.	
9	Non-irrigated agricultural lands and pastures	Areas interested by moderate agricultural activities that require tillage or pastures.	

Table 2: List of Sentinel-2 images used in the classification.

Year	No.	Sentinel Image Identification Code
2017	0	20170815T102021_20170815T102513_T31PCR
	1	20170924T102021_20170924T102649_T31PCR
	2	20170926T101009_20170926T102049_T31PCR
2018	3	20180815T102019_20180815T102918_T31PCR
	4	20180820T102021_20180820T103538_T31PCR
	5	20180911T101019_20180911T101438_T31PCR
	6	20180911T101019_20180911T102702_T31PCR
	7	20180916T101021_20180916T101512_T31PCR
	8	20180921T101019_20180921T101647_T31PCR
	9	20180924T102019_20180924T102602_T31PCR
	10	20180929T102021_20180929T103112_T31PCR
2019	11	20190812T101031_20190812T102016_T31PCR
	12	20190911T101021_20190911T102116_T31PCR
	13	20190921T101031_20190921T102426_T31PCR
	14	20190926T101029_20190926T102551_T31PCR
	15	20190929T102029_20190929T102700_T31PCR

Knowing that DOS can affect the classification's results differently depending on the geographical area (and land cover), the classification model was trained and applied over the DOS-corrected and non-corrected datasets. Then the Overall Accuracy (OA) of the classifications were compared to check the influence of DOS on the final result.

The topographical correction of the images was initially applied to reduce the effects of elevation over the plateaux areas (Dorren et al., 2003). The topographic correction allows the variation in the reflectance derived from the terrain's inclination and the sun elevation (Poortinga et al., 2019; Shepherd and Dymond, 2010). Nevertheless, the correction introduced noise in the dataset because the plateaux slopes do not interfere with the soil's spectral response. The Digital Terrain Model (DTM) applied, USGD 30m DTM, is not resolute and precise enough. Thus, the dataset was not topographically corrected.

(a)

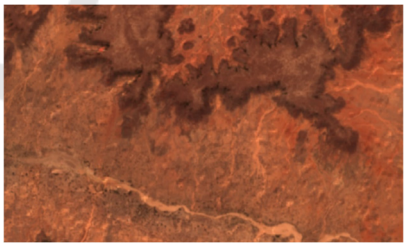

(b)

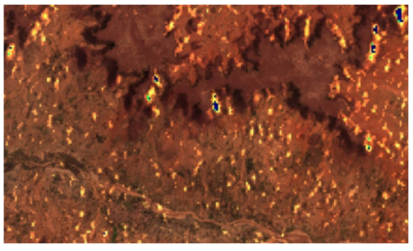

Figure 3: (a) RGB mosaic on sentinel-2, level 1C data, DOS applied; (b) RGB mosaic on sentinel 1C data, DOS applied, and topographically corrected. The correction excessively alters the data over the plateaux and the plane areas.

2.4 Features Extraction and Selection

The feature extraction consisted of the computation of 6 spectral features, 4 histogram-based features, 18 textural (computed on Sentinel band 8A), 2 elevation-derived features, and 1 edge-detector feature added to the 12 spectral bands. Specifically, the Gray Level Co-occurrence Matrix (GLCM) texture metrics were calculated over a 9x9 neighbourhood (Haralick et al., 1973), while the histogram-based features were on a 3x3 filter (Conners et al., 1984; GEE,2022) to help in classes discrimination (Drzewiecki et al., 2013; Kukawska et al., 2017). Table 3 lists the extracted features.

Table 3: Derivative features calculated for Sentinel-2.

Feature	Formula/note
Chlorophyll IndexRedEdge, CRE	(B9/B5)−1
Enhanced Vegetation Index, EVI	2.5*((B9−B5)/((B9+6*B5−7.5*B1)+1))
HUE	Arctan((2*V5−B3−B1)/30.5)*(B3−B1))
Soil Composition Index, SCI	(B11−B8)/(B11+B8)
Wetness Index, WET	(0.1509*B2)+(0.1973*B3)+(0.3279*B4)+ (0.03406*B8)-(0.7112*B11)-(0.4572*B12)
Triangular Vegetation Index, TVI	0.5*(120*(B8-B3))-(200*(B4-B3))
Sob	Sobel edge extractor
Var	Variance
Mean	Mean
Skew	Skewness
Kurt	Kurtosis
Entr	Entropy
Asm	Angular Second Moment; measures the number of repeated pairs
Corr	Correlation; measures the correlation between pairs of pixels
Var	Variance; measures how spread out the distribution of gray-levels is
Idm	Inverse Difference Moment; measures the homogeneity
Savg	Sum Average
Svar	Sum Variance
Sent	Sum Entropy
Ent	Entropy. Measures the randomness of a gray-level distribution
Dvar	Difference variance
Dent	Difference entropy
Imcorr1	Information Measure of Corr. 1
Imcorr2	Information Measure of Corr. 2
Maxcorr	Max Corr. Coefficient.
Diss	Dissimilarity
Inertia	Inertia
Shade	Cluster Shade
Prom	Cluster prominence
DSM	Digital Surface Model (NASA SRTM 30m)
Height model, HM	DSM-DTM (Global Multi-resolution Terrain Elevation 2010)

The feature selection phase is fundamental to reducing the computational time of the classification without losing accuracy (Belcore et al., 2020).

In mid-2020, the function *SmileRandomForest* was introduced in the GEE coding platform. Unlike its predecessor *RandomForest* function, it allows the computation of the layer importance, which is based on the GINI impurity system. Random Forest algorithm creates multiple decision trees (i.e. forest) using bootstrapped data samples and selects the final output based on the majority vote of the individual trees (Breiman, 2001). The Gini impurity criterion measures the purity or randomness of a set of items (Breiman, 2001). It determines the quality of a split between classes in a decision tree. The goal is to split the data in a way that results in the purest possible subset of the classes or values. The Gini impurity of a split is calculated as the sum of the probability of each class or value being incorrectly classified, given a random observation from the set. A split with a lower Gini impurity is considered a better split, as it results in a more pure subset of the classes or values. The feature that results in the lowest Gini impurity is selected as the splitting feature, and the process is repeated until a stopping criterion is reached. The GINI is calculated for each variable of the classifier. The variables with high GINI gain (so they have less impurity) are more important.

The features with less than 50 GINI gain were removed from the input dataset as resulting of an iterative comparison of 5 scenarios (Table 5). The parameters considered for the best scenario evaluation are the out-of-bag error (oob) and the overall accuracy (OA). The threshold value was selected according to the maximum accuracy achievable. Finally, the features were scaled according to their minimum-maximum values.

2.5 Classification and Multi-Temporal Strategies Comparison

The training dataset comprises 2500 points, 300 points for each class except for the urban areas class, which is constituted of 100 points. The choice of unbalancing the training is due to the low percentage of urban areas cover. Since the urban areas class covers the smallest portion of the study area and the Random Forest (RF) classifier tends to promote the more represented classes in training, few samples of the Urban areas were used to train the classifier. The validation dataset is composed of 1800 points, 200 for each class. The training and validation dataset were manually created using a 2017 map as a ground reference.

Two different multi-temporal approaches were compared: aggregated multi-temporal and stacked multi-temporal methods. In the aggregated multi-temporal, each image was separately classified using the machine learning algorithm Random Forest (RF) with 100 rifle decision trees per class and 2 as the minimum size for terminal nodes.

The same training dataset was used for each image. The results are 16 classifications that were aggregated according to the modal value. Only the more accurate classifications (equal and greater than the OA modal value) were used in the final aggregation.

Differently, the stack multi-temporal approach consisted of one classification over a dataset composed of all the features from different epochs ensembled. In this case, the images were stacked together and classified with RF algorithm (200 rifle decision trees per class and 4 as the minimum size for terminal nodes). Due to GEE's limited available memory, only 2018 and 2019 data were considered. Figure 4 shows the classification workflow.

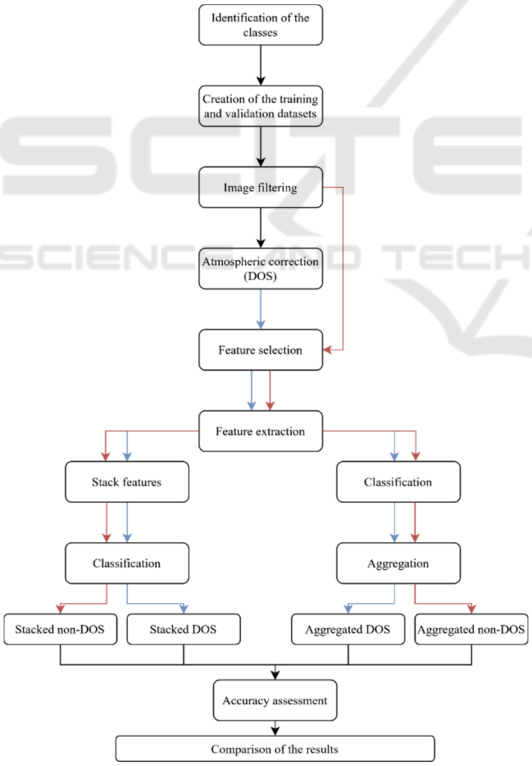

Figure 4: The workflow of the classification. Red arrows indicate the DOS processing, while the blue ones indicate the processing without DOS correction.

2.6 Accuracy Assessment

The classifications' accuracy was asses based on the error matrix-derived measures: the overall accuracy, the producer's accuracy, the user's accuracy, and the F1 score (Congalton, 1991).

2.7 Comparison to Existing LC Classifications

Today there is no official product of LC and use that can be considered a shared and trusted reference. Despite the large availability of satellite source data, no high-resolution harmonised LC product exists. In 2017 ESA created a land cover classification map of Africa at 20m resolution using 180000 Copernicus Sentinel-2 images captured between December 2015 and December 2016 (ESA, 2016). The map is still a prototype, and only eleven classes are described (i.e. Trees, Shrubs, Grasslands, Croplands, Aquatic Vegetation, Sparse Vegetation, Bare Areas, Built-Up Snow, and Open Waters). The lack of thematic detail is compensated by the 20m spatial resolution, which makes it unique in the LC data of Niger. Although it is still a partially validated prototype, it was used as reference for the validation of the LC map generated in this work with the stacked approach. The classes of the two LC systems are hardly harmonised, thus, the translation required the creation of a target shared classification for LC Africa ESA and LC of Sirba area, as Table 4 shows.

Table 4: Conversion classes between ESA Africa LC and here developed LC map.

Common classes	ESA Africa LC	Present LC
1- Vegetation	1- Trees, 2 - Shrubs, 6 - Sparse vegetation	3 - Forest and bushes, 8- Plateaux vegetation
2- Grassland	3 - Grasslands	10 – non-irrigated agricultural lands and pastures
3- Cropland	4 - Cropland	9 – Irrigated agricultural lands
4 - Bare areas	7- Bare areas	5 – Red bare soils, 6 - Sandy soils, 2 - Plateaux
5 - Built-up	8- Built-up	4 – Urban areas
6 - Waters	5 Aquatic vegetation, 10 - Open waters	1 – Water bodies

3 RESULTS

3.1 Feature Extraction and Selection

Figure 5 shows the results of the GINI importance analysis. The bands per image (initially 44) were

reduced to 16 according to the maximum achievable accuracy (Table 5) computed by considering five scenarios with reduced input features. Scenario 3 revealed better OA (0.85) and a little out-of-bag error (0.070).

Table 5: Tests run over five scenarios that differ in the number of input features in the classification selected according to their importance value (see Figure 5).

	GINI threshold	oob	OA
Scenario 1	none	0.081	0.846
Scenario 2	>40	0.069	0.846
Scenario 3	>50	0.070	0.854
Scenario 4	>60	0.084	0.849
Scenario 5	>80	0.081	0.842

3.2 Classification and Multi-Temporal Strategies Comparison

The aggregated multi-temporal classification was performed separately in 16 images with 16 features for each. Table 6 provides the OA values calculated for each classification. Classifications with OA less than 0.94 were not used for the modal aggregation. The stacked multi-temporal classification was realised using as the input dataset the features from different epochs together.

The period considered was 2018 and 2019. The input features of the stack multi-temporal classification were 76.

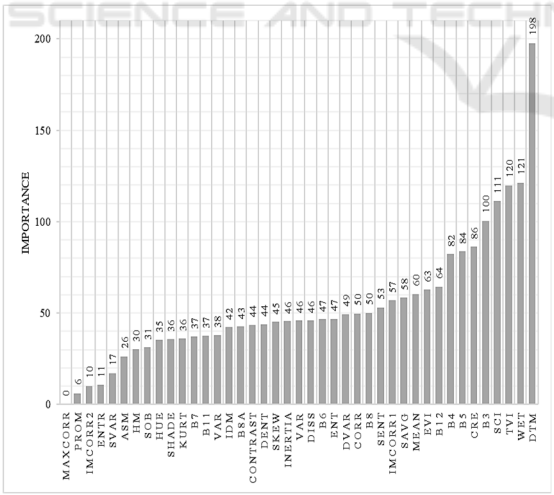

Figure 5: GINI importance (y) of the extracted features (x).

The GINI importance was computed for the 76 bands to optimise the process further. Four scenarios for the slimming out were considered (Table 7). Still, the best results in terms of OA are provided by scenario number 1, which does not remove any feature from the classification.

Table 6: OA achieved on each classification. The underlined classifications were excluded from the aggregation.

Classification no.	OA
1	0.97
2	0.95
3	0.96
4	**0.85**
5	**0.94**
6	**0.83**
7	**0.85**
8	**0.92**
9	0.95
10	0.95
11	**0.92**
12	0.95
13	0.95
14	**0.94**
15	0.95
16	0.96

Table 7: Tests run over 5 scenarios that differ in the number of input features in the classification selected according to their importance value. The parameters considered for the best scenario evaluation are the out-of-bag error (oob) and the overall accuracy (OA).

	GINI threshold	**oob**	**OA**
Scenario 1	none	0.019	0.960
Scenario 2	>9	0.020	0.958
Scenario 3	>10	0.020	0.955
Scenario 4	>20	0.023	0.951

The atmospheric correction's influence on the classifications was checked by comparing the accuracy of the same classification model applied to corrected and non-corrected input datasets. The DOS has little impact on the aggregated multi-temporal classification's goodness: it shifts the OA from 0.971 (non-corrected dataset) to 0.975 (corrected dataset). Similarly, the DOS showed little influence on the stacked method too. Indeed it shifts the OA from 0.955 (non-corrected) to 0.960 (corrected), Table 8.

Table 8: DOS influences over the classifications.

	No DOS	DOS
OA of Aggregated multi-temporal	0.971	0.975
OA of Stack multi-temporal	0.955	0.960

3.3 Accuracy Assessment

The error matrices give the performance of the classification. Both multi-temporal approaches resulted in high accuracy values. For what concerns the aggregated approach, Table 9 shows that the User's and Producer's accuracies are always above

0.95. The *Plateaux* class is less accurate, although its F1 score reaches 0.95. The model correctly identifies sandy bare soils and irrigated land classes.

Table 9: Error matrix of the aggregated multi-temporal classification.

	Water	Plateaux	Forest bushes	Urban areas	Red bare soils	Sandy bare soil	Vegetation (plateaux)	Irrigated agricultural lands	Non-irrigated lands and pastures
Water	200	0	0	0	0	0	0	0	0
Plateaux	0	189	0	0	0	0	11	0	0
Forest bushes	0	0	200	0	0	0	0	0	0
Urban areas	0	0	7	193	0	0	0	0	0
Red bare soils	0	8	0	0	188	0	0	0	4
Sandy bare soil	0	0	0	0	1	197	0	0	2
Vegetation (plateaux)	0	0	0	0	0	0	200	0	0
Irrigated agricultural lands	0	0	0	0	0	0	0	200	0
Non-irrigated lands and pastures	0	0	6	5	1	0	0	0	188
TOT	200	197	213	198	190	197	211	200	194
PA	1.00	0.96	0.94	0.98	0.99	1.00	0.94	1.00	0.97
UA	1.00	0.94	1.00	0.96	0.94	0.98	1.00	1.00	0.94
F1	1.00	0.95	0.97	0.97	0.96	0.99	0.97	1.00	0.95
OA= 0.98									

Table 10: Error matrix of the stacked multi-temporal classification.

	Water	Plateaux	Forest bushes	Urban areas	Red bare soils	Sandy bare soil	Vegetation (plateaux)	Irrigated agricultural	Non-irrigated lands and
Water	183	0	0	0	0	0	0	0	0
Plateaux	0	180	0	0	0	0	10	0	0
Forest bushes	1	0	191	0	0	0	1	3	0
Urban areas	0	0	6	161	0	0	0	0	0
Red bare soils	0	9	0	2	174	0	0	0	8
Sandy bare soil	4	0	0	0	0	178	0	0	1
Vegetation (plateaux)	0	1	0	0	0	0	195	0	0
Irrigated agricultural lands	3	0	6	0	0	0	0	171	0
Non-irrigated lands and pastures	0	0	8	4	0	0	0	0	177
TOT	191	190	211	167	174	178	206	174	186
PA	0.96	0.95	0.91	0.96	1.00	1.00	0.95	0.98	0.95
UA	1.00	0.95	0.97	0.96	0.90	0.97	0.99	0.95	0.94
F1	0.98	0.95	0.94	0.96	0.95	0.99	0.97	0.97	0.94
OA= 0.96									

Regarding the stacked classification, the accuracy values are slightly lower than the ones on the aggregate multi-temporal classification. Table 10 shows that the plateaux class reaches 0.947 of the F1-score, which is the less accurate class along the non-irrigated lands and pastures. The overall accuracy is 0.96, with only 0.05 points of difference from the aggregated methods.

Although the high accuracy value, some salt-and-pepper effect is present all over the scene; thus, some post-processing operations were carried out for aesthetic reasons. Specifically, erosion (size 4) and dilation (size 3) were realised in class *Urban areas* (Figure 6).

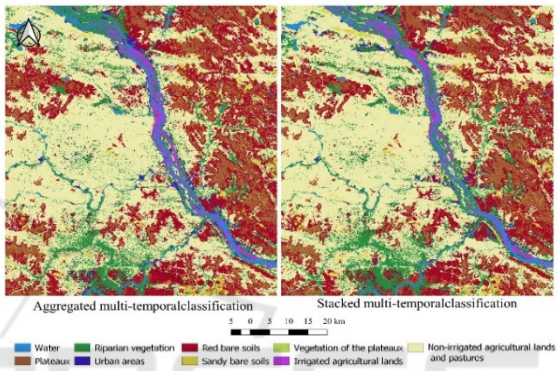

Figure 6: Example of the aggregated multi-temporal classification (left) and the stacked multi-temporal classification (right).

3.4 Comparison to Existing LC Classifications

The pixel by pixel comparison reveals an overall accuracy of 0.203 and the pixel-based confusion matrix is described in Table 11. From a visual

Table 11: Error matrix of the ESA LC Africa (reference) and Sirba Classification. To facilitate the reading, the values are reported in square kilometres.

	Vegetation	Grassland	Cropland	Bare areas	Built-up	Waters	Total
Vegetation	1068	1497	101	1568	56	97	4387
Grassland	2451	8908	105	34992	1103	787	48348
Cropland	7819	29140	1503	10711	1792	722	51686
Bare areas	36	1407	2	11037	19	113	12614
Built-up	58	4	66	59	584	12	783
Waters	10	0	101	4	0	1109	1224
Total	11442	40956	1879	58369	3554	2841	
PA	0.093	0.218	0.800	0.189	0.164	0.390	OA
UA	0.244	0.184	0.029	0.875	0.745	0.906	0.203
F1	0.135	0.200	0.056	0.311	0.269	0.546	

interpretation of the results, the water class (specifically the Sirba river) is better identified by the aggregated LC than the ESA LC (Figure 7).

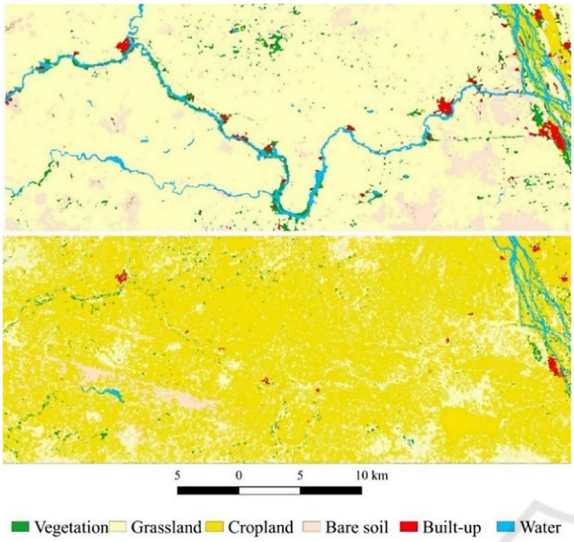

Figure 7: Sirba River area classified according Sirba LC (top) and ESA LC (bottom).

4 DISCUSSION

Both classification methods show very positive results. The little influence of DOS on the results might be caused by the short span and the very similar meteorological condition of the analysed dataset. Also, the RF, which is slightly sensitive to non-normalised datasets, might contribute to such results. Although DOS has little influence on the results, it was maintained in the classification workflow because of its lightweight processing time. More complex atmospheric correction models can require more computational power and processing time. Thus, further and more detailed analysis needs to be realised in this direction.

The GINI importance analysis allows the lightening of the classification process and improves the classification's performance. Although this was not true for the stacked classification, reducing the dataset reduces the OA. It is worth underlining that the importance analysis was applied twice in this case. The DOS correction has little influence on the final accuracy results for both multi-temporal approaches. This is an unexpected result since most relevant literature underlines the importance of atmospheric correction in multi-temporal approaches, especially in stacked ones.

Little distance also emerges from the comparison of the two multi-temporal approaches. The aggregated multi-temporal classification overcomes the stacked one for only 0.015 of OA (regardless of the atmospheric correction). The F1 score of some classes of the aggregated multi-temporal approach is 1 (water and irrigated lands). In the stacked multi-temporal approaches, the F1 score shows some differences: irrigated land class is not one of the most accurate classes, but bare soil is. This method seems to misclassify the irrigated class, which is often confused with forest or water. Despite some little differences, in this case, the two approaches are perfectly exchangeable for this specific application. Again, there is a little difference in terms of time to apply one or the other.

Nevertheless, there is a strong possibility of running out of memory in additional features or a vast area. Indeed data from 2017 were taken out. In this specific application, the aggregated multi-temporal classification method was applied because of the slightly higher accuracy and the less scarcity of salt-and-pepper effect all over the scene.

The pixel-by-pixel comparison between the LC ESA map and the aggregated LC reveals low overall accuracy (0.203) despite the two classifications having similar spatial resolutions (10m and 20m). The primary issue regards the confusion between *Grassland*, *Cropland* and *Bare areas*. Most pixels classified as *Grassland* in Sirba LC are considered *Bare areas* in the ESA Africa LC (Table 11). Similarly, most of the croplands of the Sirba LC are classified as *Grassland* in the ESA LC. Indeed the F1 score of *Cropland* is only 0.056. Such results are ascribable to the nature of the definitions of pastures, grasslands and bare soils. In fact, pastures are considered *Agricultural land* in ESA LC and *Grassland* in Sirba LC. This is clearly detectable from the visual comparison between the classifications (Figure 7). Sirba River and most seasonal ponds and lakes are detected in Sirba LC and not in ESA LC because of the dataset of the classifications. Sirba LC is a rainy season LC (only summer months in 2017-2019), while ESA LC is based on one-year observations. This also influences the vegetation class, which is captured at its maximum during the rainy season. A good overlap is present between the other classes. It is worth underling that the ESA Africa LC is a prototype, and it was validated using Crowdsourcing only for Kenya, Gabon, Ivory Coast and South Africa. The analysis and the methodology applied for the classification demonstrate that the textural information facilitates segmentation and classification.

Similarly, the aggregated multi-temporal approach proposed to reduce the variability of the images led to high-accuracy classification. Selecting a limited period for the satellite classification allowed the maximisation of the seasonal characterisation. It increased the separability of some hard-to-map classes (e.g. Nigerienne urban areas from bare soils and pastures and water).

5 CONCLUSIONS

Regardless of the application of atmospheric correction, the classification provides a suitable LC map for flood planning. It follows that, with some specific actions, it is possible to overcome the main mapping difficulties and obtain LC maps with high thematic detail in sub-Saharan areas. The model proposed in this paper can be applied to classify other sub-Saharan river areas semi-automatically since it is developed in GEE.

REFERENCES

Anadia 2.0. climateservices.it CNR-IBE. URL https://climateservices.it/progetto/anadia/ (accessed 2.8.23).

Belcore, E., Piras, M., Pezzoli, A., 2022. Land Cover Classification from Very High-Resolution UAS Data for Flood Risk Mapping. Sensors 22, 5622. https://doi.org/10.3390/s22155622

Belcore, E., Piras, M., Wozniak, E., 2020. Specific alpine environment land cover classification methodology: Google Earth Engine processing for Sentinel-2 data, in: Volume XLIII-B3-2020. Copernicus Publications, pp. 663–670. https://doi.org/10.5194/isprs-archives-XLIII-B3-2020-663-2020

Bigi, V., Pezzoli, A., Rosso, M., 2018. Past and Future Precipitation Trend Analysis for the City of Niamey (Niger): An Overview. Climate 6, 73. https://doi.org/10.3390/cli6030073

Breiman, L., 2001. Random Forests. Machine Learning 45, 5–32. https://doi.org/10.1023/A:1010933404324

Chavez, P.S., 1988. An improved dark-object subtraction technique for atmospheric scattering correction of multispectral data. Remote Sensing of Environment 24, 459–479.https://doi.org/10.1016/0034-4257(88)90019-3

Congalton, R.G., 1991. A review of assessing the accuracy of classifications of remotely sensed data. Remote Sensing of Environment 37, 35–46. https://doi.org/10.1016/0034-4257(91)90048-B

Conners, R. W., Trivedi, M.M., Harlow, C.A., 1984. Segmentation of a high-resolution urban scene using texture operators. Computer Vision, Graphics, and Image Processing 25, 273–310. https://doi.org/10.1016/0734-189X(84)90197-X

Dorren, L.K.A., Maier, B., Seijmonsbergen, A.C., 2003. Improved Landsat-based forest mapping in steep mountainous terrain using object-based classification. Forest Ecology and Management 183, 31–46. https://doi.org/10.1016/S0378-1127(03)00113-0

Drzewiecki, W., Wawrzaszek, A., Aleksandrowicz, S., Krupiński, M., Bernat, K., 2013. Comparison of selected textural features as global content-based descriptors of VHR satellite image, in: 2013 IEEE International Geoscience and Remote Sensing Symposium - IGARSS. Presented at the 2013 IEEE International Geoscience and Remote Sensing Symposium - IGARSS, pp. 4364–4366. https://doi.org/10.1109/IGARSS.2013.6723801

ESA, 2016. ESA CCI LAND COVER – S2 prototype Land Cover 20m map of Africa 2016 [WWW Document]. URL http://2016africalandcover20m.esrin.esa.int/ (accessed 4.12.21).

GEE, n.d. Google Earth Engine [WWW Document]. URL https://earthengine.google.com/platform/ (accessed 3.9.20).

Haralick, R.M., Shanmugam, K., Dinstein, I., 1973. Textural Features for Image Classification. IEEE Transactions on Systems, Man, and Cybernetics SMC-3, 610–621. https://doi.org/10.1109/TSMC.1973.4309314

Huete, A. R., 1988. A soil-adjusted vegetation index (SAVI). Remote Sensing of Environment 25, 295–309. https://doi.org/10.1016/0034-4257(88)90106-X

Kukawska, E., Lewiński, S., Krupiński, M., Malinowski, R., Nowakowski, A., Rybicki, M., Kotarba, A., 2017. Multitemporal Sentinel-2 data - remarks and observations, in: 2017 9th International Workshop on the Analysis of Multitemporal Remote Sensing Images (MultiTemp). Presented at the 2017 9th International Workshop on the Analysis of Multitemporal Remote Sensing Images (MultiTemp), pp. 1–4. https://doi.org/10.1109/Multi-Temp.2017.8035212

Lantzanakis, G., Mitraka, Z., Chrysoulakis, N., 2017. Comparison of Physically and Image Based Atmospheric Correction Methods for Sentinel-2 Satellite Imagery, in: Karacostas, T., Bais, A., Nastos, P.T. (Eds.), Perspectives on Atmospheric Sciences, Springer Atmospheric Sciences. Springer International Publishing, pp. 255–261.

Li, Q., Qiu, C., Ma, L., Schmitt, M., Zhu, X.X., 2020. Mapping the Land Cover of Africa at 10 m Resolution from Multi-Source Remote Sensing Data with Google Earth Engine. Remote Sensing 12, 602. https://doi.org/10.3390/rs12040602

Massazza, G., Tamagnone, P., Pezzoli, A., Housseini, M., Belcore, E., Tiepolo, M., Rosso, M., 2018. Améliorations sur le système d'observation du bassin de la Rivière Sirba pour la gestion des risques naturels, in: Colloque International AMMA-CATCH. AMMA CATCH.

Massazza, G., Tamagnone, P., Wilcox, C., Belcore, E., Pezzoli, A., Vischel, T., Panthou, G., Housseini Ibrahim, M., Tiepolo, M., Tarchiani, V., Rosso, M., 2019. Flood Hazard Scenarios of the Sirba River

(Niger): Evaluation of the Hazard Thresholds and Flooding Areas. Water 11, 1018. https://doi.org/10.3390/w11051018

Oguntunde, P.G., Lischeid, G., Abiodun, B.J., 2018. Impacts of climate variability and change on drought characteristics in the Niger River Basin, West Africa. Stoch Environ Res Risk Assess 32, 1017–1034. https://doi.org/10.1007/s00477-017-1484-y

Poortinga, A., Tenneson, K., Shapiro, A., Nquyen, Q., San Aung, K., Chishtie, F., Saah, D., 2019. Mapping Plantations in Myanmar by Fusing Landsat-8, Sentinel-2 and Sentinel-1 Data along with Systematic Error Quantification. Remote Sensing 11, 831. https://doi.org/10.3390/rs11070831

Shepherd, J. D., Dymond, J.R., 2010. Correcting satellite imagery for the variance of reflectance and illumination with topography. International Journal of Remote Sensing. https://doi.org/10.1080/01431160210154029

Tamagnone, P., Massazza, G., Pezzoli, A., Rosso, M., 2019. Hydrology of the Sirba River: Updating and Analysis of Discharge Time Series. Water 11, 156. https://doi.org/10.3390/w11010156

Teodoro, A.C., Duarte, L., 2022. Chapter 10 - The role of satellite remote sensing in natural disaster management, in: Denizli, A., Alencar, M.S., Nguyen, T.A., Motaung, D.E. (Eds.), Nanotechnology-Based Smart Remote Sensing Networks for Disaster Prevention, Micro and Nano Technologies. Elsevier, pp. 189–216. https://doi.org/10.1016/B978-0-323-91166-5.00015-X

Tiepolo, M., Bacci, M., Braccio, S., 2018. Multihazard Risk Assessment for Planning with Climate in the Dosso Region, Niger. Climate 6, 67. https://doi.org/10.3390/cli6030067